CHAPTER VII

OPTICAL MULTIMODE INTERFERENCE WAVEGUIDES AS SENSING DEVICES

DOI: 10.51859/amplla.sst631.1122-7

Yuri Hayashi Isayama [1]
Jhonattan Cordoba Ramirez [2]
Lucas Heitzmann Gabrielli [3]
Hugo Enrique Hernández-Figueroa [4]

[1] PhD in Electrical Engineering from University of Campinas - UNICAMP
[2] Assistant Professor at the School of Engineering. Federal University of Minas Gerais - UFMG
[3] Associate Professor at the School of Electric and Computer Engineering. University of Campinas - UNICAMP
[4] Full Professor at the School of Electric and Computer Engineering. University of Campinas - UNICAMP

ABSTRACT

Optical interferometers are important and versatile building blocks in integrated optics. They can present a wide variety of operating mechanisms and have several distinct applications, where one of them is optical sensing. The multimode interferometer (MMI) is an established structure but has only recently received attention as a sensing device. These devices can be designed to be compact, highly sensitive and present fast response times, which led them to be explored as refractive index sensors. Most recently, due to this high sensitivity and real-time monitoring capabilities, in addition to the possibility for dense integration, MMI sensors were intensively investigated for biosensing applications. The first MMI sensors were simple in construction, as they operated only with the first two propagating modes of a multimode waveguide. As higher order modes were employed, significant gains in sensor performance were achieved, but the device also grew in complexity. This chapter aims to provide a short history of MMI sensors, present the theory behind its operation (multimode waveguide design, device excitation and detection methods) and recent advances both in theoretical modeling and experimental demonstrations.

Key words: Integrated optics. Multimode interference. Modal interferometer. Sensor. Optical waveguide devices.

1. INTRODUCTION

Interferometers belong to one of the most important class of devices for many areas such as telecommunications (WILKES *et al*., 2016; CHILES; FATHPOUR, 2014; YURTSEVER *et al.*, 2014; FANDIÑO; MUÑOZ, 2013), sensing (ZINOVIEV *et al*., 2011; GONZÁLEZ-GUERRERO *et al*., 2017; ESTEVEZ; ALVAREZ; LECHUGA, 2012; KOZMA *et al.*, 2014) and other applications in fundamental physics (CRESPI *et al.*, 2013; BERRADA *et al.*, 2013). Progress and developments in the field of photonic sensors, with the implementation of a variety of devices, such as ring resonators and interferometers, have allowed the production of sensing devices characterized by compactness, high sensitivity (with limit of detection between 10^{-6} and 10^{-8} refractive index units – RIU), very fast response times, label-free and real-time monitoring capabilities (GAVELA *et al*., 2016) in applications related to sensing and biosensing. In this context, Multimode Interference (MMI) sensors have received plenty of attention over the last decades.

The first suggestions of the use of planar multimode waveguides as multimode interferometers arose during the 1970s (ULRICH, 1975). Throughout the 1990s, several possible applications for this type of structure were idealized, such as couplers (SOLDANO; PENNINGS, 1995; SOLDANO *et al*., 1992), filters (LEUTHOLD et al., 1996), modal converters (LEUTHOLD *et al*., 1998), and power splitters (RASMUSSEN; RASMUSSEN; POVLSEN, 1995; LEUTHOLD; JOYNER, 2001; SOLDANO; PENNINGS, 1995). In the 2000s, works regarding MMI were no longer limited to planar waveguides, also including proposals and demonstrations of the same applications utilizing optical fibers (MOHAMMED; MEHTA; JOHNSON, 2004; MOHAMMED; SMITH; GU, 2006; ANTONIO-LOPEZ *et al*., 2010).

The first use of a MMI with a sensing function was proposed by Gut *et al.* in 1999 (GUT *et al.*, 1999). This work demonstrated both theoretically and experimentally how the interaction between fundamental and first order Transverse Electric (TE) modes could be utilized for gas detection. In addition, it also suggested the possibility of using fundamental TE and Transverse Magnetic (TM) modes with the same purpose, without, however, the experimental demonstration. From this point, many other attempts to expand this initial proposition arose, both as planar MMI waveguides (SOLER *et al*., 2020; ELSAYED *et*

al., 2017), as well as fiber optics MMI (MEHTA; MOHAMMED; JOHNSON, 2003; MOHAMMED; SMITH; GU, 2006; WANG; FARRELL, 2006; ANTONIO-LOPEZ *et al*., 2010).

Regarding planar MMI waveguide sensors, the main contributions are basically divided in sensors called bimodal (Bimodal Waveguide - BiMW) and trimodal (Trimodal Waveguide - TriMW), which have both theoretical and experimental demonstrations. Recently, there were also theoretical proposals of MMI sensors that operated with high order modes. The main difference between these types of sensors are the interfering modes excited within the multimode waveguide: bimodal sensors operate with fundamental and first order modes, trimodal sensors operate with fundamental and second order modes, and high order sensors use the fundamental and a higher order (third and above) mode.

In 2005, Kribich *et al.* demonstrated the use of a MMI as a humidity sensor and suggested, for the first time, that this device could be used in the future as a biosensing device (KRIBICH *et al.*, 2005). From this point on, most advancements in MMI sensing technology were directed towards biosensing applications, exemplified by Zinoviev *et al.* in 2011, where an experimental demonstration of a MMI biosensor was developed, detecting BSA (Bovine Serum Albumin) protein (ZINOVIEV *et al*., 2011). The limit of detection (LOD) for this device was estimated as LOD = 2.5×10^{-7} Refractive Index Unit (RIU). The sensing device consisted of a MMI that supported the first two TE propagating modes and it was denominated Bimodal Waveguide (BiMW) biosensor.

Attempting to improve device sensitivity, different proposals were developed altering MMI geometry (EBIHARA; ASAKAWA; SUZUKI, 2021, TORRIJOS-MORÁN *et al*., 2021, TSAREV, 2021), mode excitation (HOPPE *et al*., 2017, LIANG et al., 2018, EBIHARA et al., 2019), in-chip light coupling (GRAJALES *et al*., 2019), MMI materials (DWIVEDI; KUMAR, 2017), sensor detection methods (DWIVEDI; KUMAR, 2018), and mode order within the MMI (RAMIREZ *et al*., 2015, GAVELA *et al*., 2016, RAMIREZ *et al*., 2019, ISAYAMA; HERNÁNDEZ-FIGUEROA, 2021). In the context of biosensing applications, several advancements were made, such as Lab-on-a-chip demonstrations (DUVAL *et al*., 2012, MALDONADO *et al*., 2020) and detection of biomolecules in solutions as blood (KIM *et al.*, 2017) and urine (GONZÁLEZ-GUERRERO *et al*., 2017).

2. MULTIMODE WAVEGUIDE INTERFERENCE (MMI) SENSOR

The basic operating principle of MMI sensors consists of comparing how the fundamental mode and a higher order mode respond to variations in the cladding layer of the sensing waveguide. If the higher order mode of the MMI sensor is the first order mode, it is denominated bimodal waveguide (BiMW) sensor and if the higher order mode is the second order, than it is called trimodal waveguide (TriMW) sensor. Initially, since the fundamental mode and the higher order mode have different propagation constants (β), a phase shift will be observed between them at the end of the multimode waveguide (MMW). Then, because the Electromagnetic (EM) field distribution of each mode is different, altering the constitution (i.e., the refractive index) of the cladding will result in different variations in each mode's β. By knowing how the two propagating modes will behave with this change in the cladding and measuring how much the phase difference between the two modes has been altered, it is, therefore, possible to evaluate the variation in the refractive index of the cladding with high precision. If the sensing waveguide is subject to biofuncionalization, this interferometer may be employed as a biosensing device.

2.1. DESIGN PROCEDURE AND IMPORTANT PARAMETERS

When designing a MMI sensor and trying to optimize its sensitivity, one fundamental factor should be considered: the device operates fundamentally by comparing the propagation constants of two given modes and, hence, it is reasonable to assume that the bigger the $\Delta\beta = \beta_{00} - \beta_{0n}$ (where β_{00} and β_{0n} are the propagation constants of the fundamental and the high-order mode, respectively) the more sensitive the device should be. If $\Delta\beta$ is naturally large, it means both propagating modes present very different guiding regimes, that is, one mode interacts more with variations in the cladding than the other (ISAYAMA; HERNÁNDEZ-FIGUEROA, 2021).

To properly design a MMI sensor, one must choose the geometry of the MMW and the operating modes in a way that maximizes the amount of the EM fields of the higher order mode in the cladding region. Figure 1 shows the MMW cross-section, where the waveguide's core height and width are denoted by h and w, respectively. For each combination of h and w chosen, the propagation constants of the modes are calculated, as exemplified in Figure 2 (assuming a Si3N4 (n_{Si3N4} = 2.0394)

channel waveguide, for operation in 633 nm wavelength, with core height (h) of 150 nm, SiO2 substrate (n_{SiO2} = 1.4570) and a cladding with refractive index n_{clad} = 1.32).

Figure 1 – Cross-section view of the multimode waveguide. The waveguide's core height and width are denoted by h and w, respectively. The propagation is assumed to be in the z-direction. Reproduced with permission from Isayama, Y.H. and Hernández-Figueroa, H.E., published by Sensors, 2021.

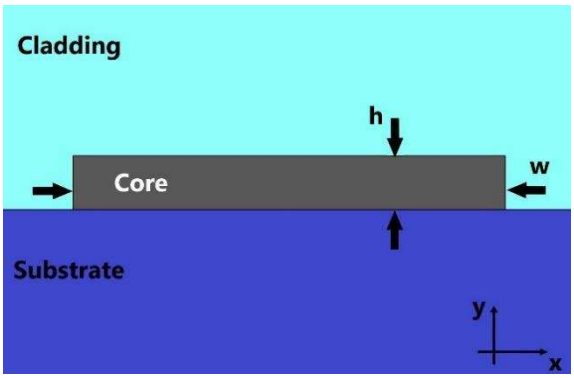

Source: ISAYAMA, Y. H.; HERNÁNDEZ-FIGUEROA, H.E. High-order multimode waveguide interferometer for optical biosensing applications. Sensors, v. 21(9), 2021.

The waveguide's core height (h) is fixed, the width (w) is varied, and the propagation constants of the modes are calculated. The solid lines are the curves for TE modes and the dashed lines are for TM modes. Due to the aspect ratio of the waveguide (width of the core much larger than its height), TM modes present much smaller propagation constants, as the modes are not well-confined in the core and much of their power propagates through both the cladding and the substrate. For TE modes, however, it is interesting to note that, if we compare the fundamental TE mode (TE_{00} in Figure 2) with other higher-order TE_{0n} modes when they are close to cutoff condition, as we increase the order of the mode, or the value of n, larger values for $\Delta\beta(w = w_{cutoff})$ are obtained. There is, naturally, a limit to this increase, since the value of β_{00} cannot grow indefinitely, which suggests there is an optimal mode order for each waveguide height design. Employing further higher-order modes will not bring any improvements in terms of device sensitivity (ISAYAMA; HERNÁNDEZ-FIGUEROA, 2021).

Figure 2 – Propagation constants for TE and TM modes of a Si3N4 channel waveguide with h = 150 nm, SiO2 substrate and nclad = 1.32. Reproduced with permission from Isayama, Y.H. and Hernández-Figueroa, H.E., published by Sensors, 2021.

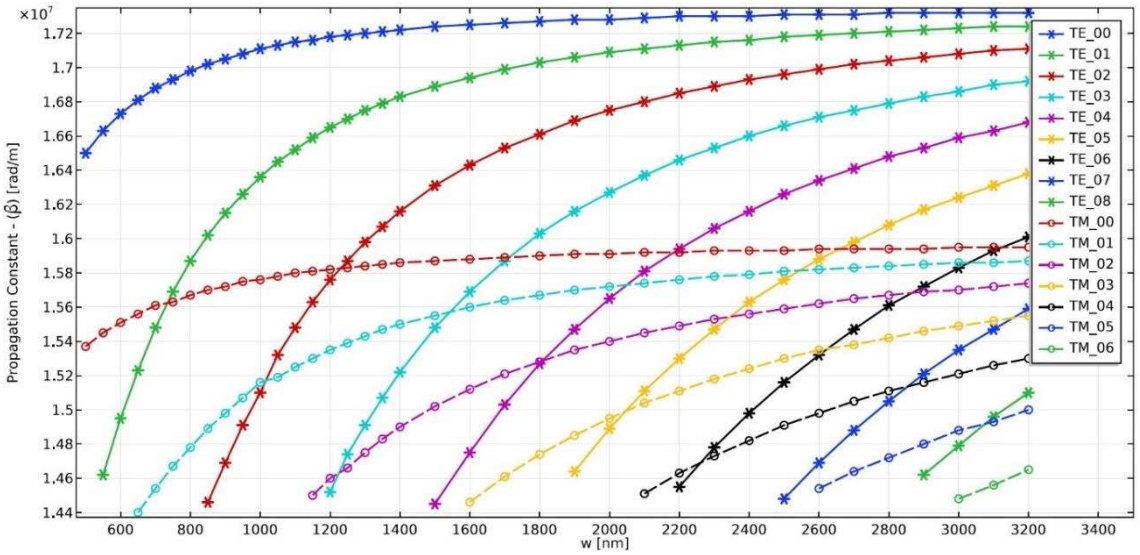

Source: ISAYAMA, Y. H.; HERNÁNDEZ-FIGUEROA, H.E. High-order multimode waveguide interferometer for optical biosensing applications. Sensors, v. 21(9), 2021.

Another important aspect to be considered is the distribution of power in the core, cladding, and substrate (P_{core}, P_{clad} and P_{subs}, respectively). The time average of the power flow through a surface S is given by

$$P_S = \iint_S \frac{1}{2} Re\{(\mathbf{E} \times \mathbf{H}^*) \cdot \mathbf{u}_z\} dS, \quad (1)$$

where $\mathbf{E}$ is the electric field, $\mathbf{H}^*$ is the complex conjugate of the magnetic field, and $\mathbf{u}_z$ denotes a unit vector in the z-direction (which is assumed to be the direction of propagation, perpendicular to the surface S). The surface S can be any of the regions: core, cladding, or substrate. Calculating the power flow in each region, one can obtain the power distribution by evaluating

$$P_{Region}[\%] = \frac{P_A}{P_{total}} \times 100\%, \quad (2)$$

where P_A denotes the power calculated by Equation (1) in the core, cladding, or substrate and P_{total} denotes the total power. Results for the example of Figure 2 are shown in Table 1.

Table 1 – Power distribution for TE_{0n} modes, for Si3N4 channel waveguide with h = 150 nm. Reproduced with permission from Isayama, Y.H. and Hernández-Figueroa, H.E., published by Sensors, 2021.

Mode Number (n)	**w [nm]**	**P_{core} TE_{00} [%]**	**P_{core} TE_{00} [%]**	**P_{core} TE_{00} [%]**
0	600	69.4	13.1	17.5
0	900	70.9	12.2	16.9
0	1300	71.4	11.9	16.7
0	1600	71.5	11.9	16.7
0	1900	71.5	11.8	16.6
0	2200	71.6	11.8	16.6
0	2500	71.6	11.8	16.6
0	2900	71.6	11.8	16.6
Mode Number (n)	w [nm]	P_{core} TE_{00} [%]	P_{core} TE_{00} [%]	P_{core} TE_{00} [%]
1	600	56.1	20.7	23.2
2	900	56.0	20.0	24.0
3	1300	61.7	15.6	22.7
4	1600	62.1	15.8	22.0
5	1900	62.1	15.8	22.1
6	2200	61.6	15.6	22.8
7	2500	60.5	15.2	24.4
8	2900	64.8	15.0	20.2

Source: ISAYAMA, Y. H.; HERNÁNDEZ-FIGUEROA, H.E. High-order multimode waveguide interferometer for optical biosensing applications. Sensors, v. 21(9), 2021.

Even though we observe from Figure 2 that $\Delta\beta$ increases until mode TE_{07} and, thus, an increase in sensitivity is expected, from Table 1, we draw different conclusions. Most of the power of the fundamental TE mode is concentrated in the core of the waveguide, and for higher-order TE modes, less of the power is inside the core. The issue is that a large part of the outside power is concentrated in the substrate, with no use for the sensing device. In fact, the amount of power in the substrate is actually larger than the portion in the cladding. One must optimize the combination of dimensions h and w and find the high order mode that produces large $\Delta\beta$ (which can be achieved by delocalizing the higher order modes from the core or increasing confinement of the fundamental mode) while also having power majorly concentrated in the cladding region.

2.2. BULK SENSITIVITY CALCULATIONS

Once the more fundamental aspects of the MMI sensor were addressed, the next step is to calculate the device's sensitivity. The bulk sensitivity is related to the

effective index variation of the interfering modes when subject to a bulk change in the refractive index of the sensing region of the interferometer. In other words, variations in the sensing region's refractive index cause the effective indexes of the interfering modes to change, which, in turn, cause a phase difference between the two of them to arise at the end of the interferometric region. This phase difference ($\Delta\phi$) may be calculated by

$$\Delta\phi = \frac{2\pi\Delta n_{eff}L}{\lambda} \tag{3}$$

$$\Delta n_{eff} = n_{eff,n} - n_{eff,0} \tag{4}$$

where $n_{eff,n}$ is the effective index of the n^{th} order mode (n = 1 for the BiMW and n = 2 for the TriMW), $n_{eff,0}$ is the effective index of the fundamental mode, L is the length of the interferometer sensing area, and λ is the vacuum wavelength at the operating frequency. Then, the bulk sensitivity can be calculated by

$$S_{bulk} = \frac{\partial(\Delta\phi)}{\partial n_{clad}} = \frac{2\pi L}{\lambda}\eta_{bulk} \tag{5}$$

$$\eta_{bulk} = \frac{\partial(\Delta n_{eff})}{\partial n_{clad}}, \tag{6}$$

where n_{clad} is the refractive index of the cladding. The parameter η_{bulk} is called intrinsic bulk sensitivity. Since the MMI interference sensor's sensitivity is dependent on the device's length (L), η_{bulk} is a good comparative parameter for different sensors within this technology.

Using Equations (3)-(6), one may calculate the intrinsic bulk sensitivity for an MMI sensor. Figure 3 shows the obtained values of η_{bulk} as a function of n_{clad} for a Si_3N_4 channel waveguide with h = 300 nm.

It is observed that the 4^{th} order MMI sensor presented the highest intrinsic bulk sensitivity of all designs for practically all values of n_{clad}. In addition, it can be pointed out how η_{bulk} decreased for mode orders superior to 4, which tells us that simply increasing mode order does not necessarily result in a performance improvement for this type of sensor.

Figure 3 – Intrinsic bulk sensitivity as a function of nclad for Si3N4 channel waveguides with h = 300 nm. Reproduced with permission from Isayama, Y.H. and Hernández-Figueroa, H.E., published by Sensors, 2021.

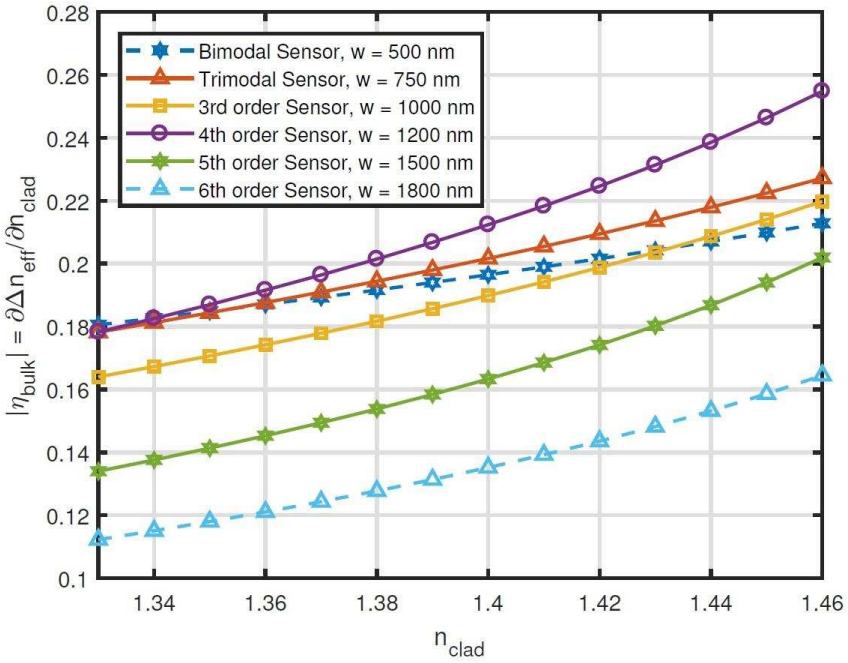

Source: ISAYAMA, Y. H.; HERNÁNDEZ-FIGUEROA, H.E. High-order multimode waveguide interferometer for optical biosensing applications. Sensors, v. 21(9), 2021.

Finally, a good metric to compare the presented sensor with other devices from other technologies is the limit of detection (LOD), which represents the smallest variation in the refractive index of the cladding that could be measured, and can be calculated by

$$\mathrm{LOD} = \frac{3 \cdot \mathrm{N/S}}{\mathrm{S_{bulk}}}, \tag{7}$$

where N/S is the noise-to-signal ratio. In practical terms, a good MMI sensor requires not only high S_{bulk}, but it also depends on the experimental setup, which affects the value of N/S.

3. MULTIMODE WAVEGUIDE INTERFERENCE EXCITATION SCHEMES

After establishing how the design of the multimode waveguide is to be developed, the next step is to determine how the desired modes are to be excited within the MMI. There are two requirements for this matter: exciting the fundamental and high order modes, while guaranteeing that these are the sole propagating modes within the multimode waveguide (sensing region) of the sensor

and obtaining an equal input power distribution between the modes (ISAYAMA; HERNÁNDEZ-FIGUEROA, 2021).

3.1. SINGLE-MODE WAVEGUIDE WITH ABRUPT TRANSITION (STEP JUNCTION)

For the BiMW and TriMW, both fundamental and high order modes can be excited through an abrupt transition (step junction) from a single-mode waveguide to the multimode waveguide, as illustrated in Figure 4. The butt-coupling coefficients (c_n) determine how the mode from the input single-mode waveguide (E,H) will couple to each propagating mode of the MMI (e_n,h_n):

$$c_n = \frac{\iint_S \mathbf{E}\times\mathbf{h_n}\cdot d\mathbf{S}}{\iint_S \mathbf{e_n}\times\mathbf{h_n}\cdot d\mathbf{S}} \tag{8}$$

Figure 4 – Scheme of the Trimodal waveguide sensor showing the expected light modes in each section. Reproduced with permission from Ramirez, J. C., published by Sensors, 2019.

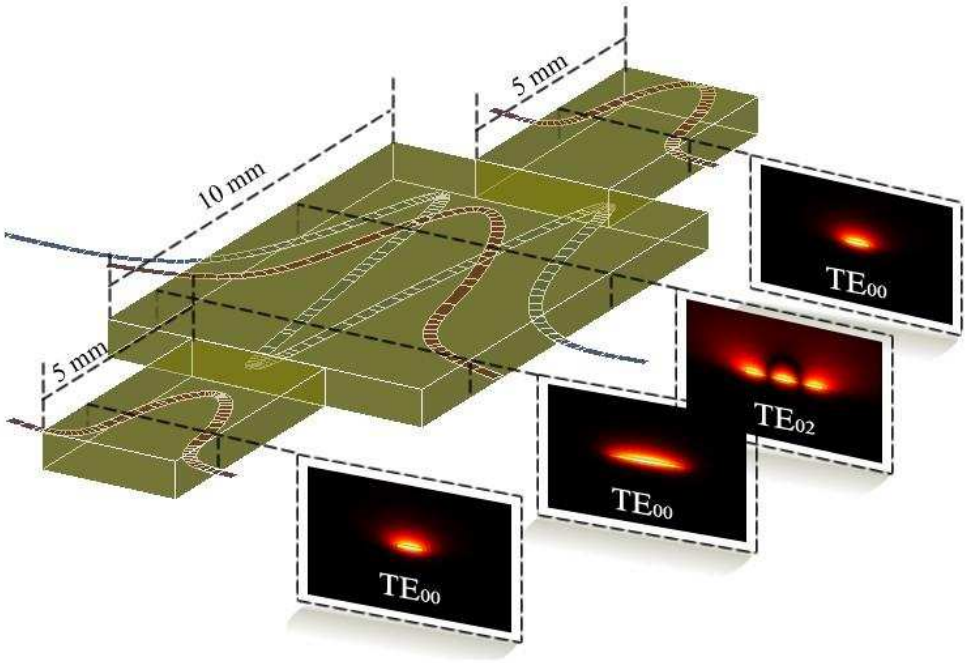

Source: RAMIREZ, J. C. et al. Trimodal waveguide demonstration and its implementation as a high order mode interferometer for sensing application. Sensors (Basel), v. 19, n. 12, p. 2821, 6 2019.

For the BiMW, because the MMI only supports two propagating modes, if there is an offset between the input single-mode waveguide and the MMI, both the fundamental and the first order modes will be excited. The optimization of the excitation structure will determine the width of the input waveguide and the offset that produces the desired excitation.

In the case of the TriMW, to ensure the sole propagation of the fundamental and second order mode, the input single-mode waveguide must be positioned at the

center of the MMI. From Equation 8, because the first order mode in the MMI presents odd symmetry, if the input waveguide is connected to the center of the multimode waveguide, the coupling coefficient (c_1) goes to zero. Then, the parameters to be optimized is only the input single-mode waveguide width.

For higher order MMI sensors, the abrupt transition will not guarantee that only the two desired modes propagate and, therefore, a different excitation scheme is necessary.

3.2. BUTT-COUPLING AND DIRECTIONAL COUPLING

The step junction from single-mode to multimode waveguide depicted in Figure 4 is simple to implement but has two major drawbacks: it is not adequate for exciting MMI sensors of order higher than the second and it does not provide fine control over power distribution between excited modes. To solve these issues, a mixed approach can be employed, by exciting the fundamental mode through butt-coupling effect and the higher order mode through directional coupling mechanism (ISAYAMA; HERNÁNDEZ-FIGUEROA, 2021).

Using Equation 8, one or more input waveguides may be designed to excite the fundamental mode in the MMI through butt-coupling (BC-SMW – Butt-coupling single-mode waveguide). The idea is to produce an EM field distribution that is very similar to the EM field distribution of the fundamental mode of the multimode waveguide so the value of c_0 (fundamental mode coupling coefficient) is maximized, while minimizing the values of c_1, c_2, c_3, etc.

The excitation of the high order mode is realized through directional coupling: if the desired mode has even symmetry, then a couple of additional waveguides is needed; if the desired mode has odd symmetry, only one additional waveguide is necessary. The new single-mode waveguides (DC-SMW – Directional coupling single-mode waveguide) are designed to satisfy the phase matching condition, meaning the propagation constant of the fundamental mode of the DC-SMW should be the same as the propagation constant of the high order mode within the MMI. This will result in the sole excitation of the desired mode, without the presence of other undesired modes. An example of such structure is shown in Figure 5, where w_{SMW} is the width of both BC-SMWs and DCSMWs, w_{MMW} is the width of the MMW sensor, g_1 is the gap between the DC-SMW and the MMW, g_2 is the separation between the BC-SMWs, $L_{BC\text{-}SMW}$ is the length of the BC-SMWs, and L_{DC} is the length

where the DC-SMWs couple to the MMW (the total length of the DC-SMW is $L_{BC\text{-}SMW}$ +L_{DC}). The values of w_{MMW}, g_1, g_2, $L_{BC\text{-}SMW}$, and L_{DC} should be optimized to produce the sole excitation of fundamental and higher order modes in the MMI, while also providing the same power distribution in both. Figure 6 shows simulation results for the excitation of a 4th order MMI sensor (ISAYAMA; HERNÁNDEZ-FIGUEROA, 2021).

Figure 5 – BC-SMW/DC-SMW excitation scheme. w_{SMW} is the width of both BC-SMWs and DCSMWs, w_{MMW} is the width of the MMW sensor, g_1 is the gap between the DC-SMW and the MMW, g_2 is the separation between the BC-SMWs, $L_{BC\text{-}SMW}$ is the length of the BC-SMWs, and L_{DC} is the length where the DC-SMWs couple to the MMW (the total length of the DC-SMW is $L_{BC\text{-}SMW}$ +L_{DC}). Reproduced with permission from Isayama, Y.H. and Hernández-Figueroa, H.E., published by Sensors, 2021.

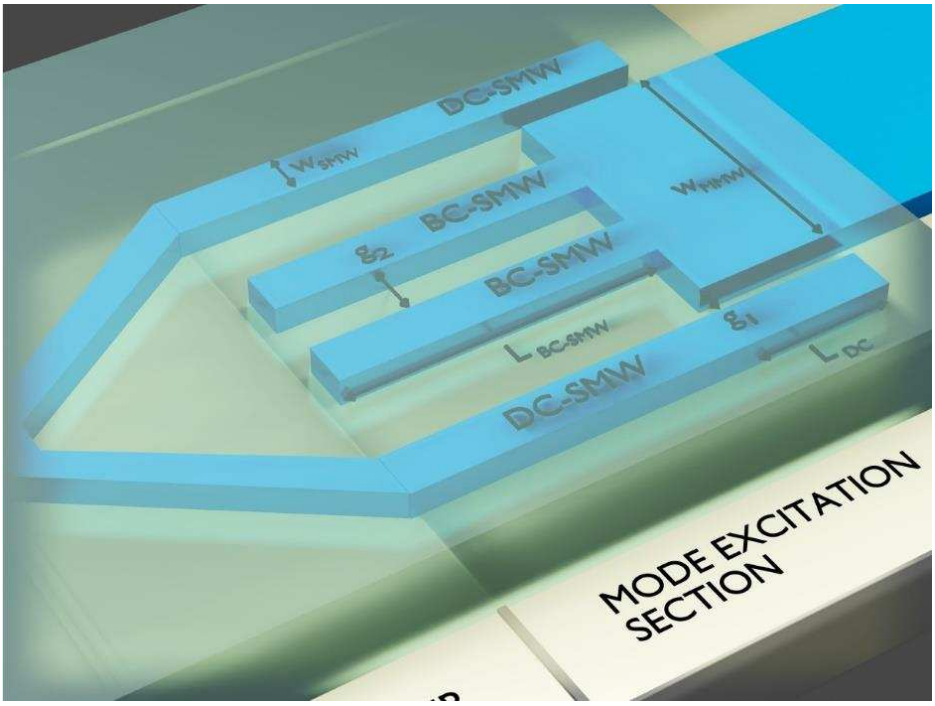

Source: ISAYAMA, Y. H.; HERNÁNDEZ-FIGUEROA, H.E. High-order multimode waveguide interferometer for optical biosensing applications. Sensors, v. 21(9), 2021.

Figure 6 – Electric field distribution (E_x component) for the simulated 4th order Si_3N_4 MMW. (a) Simulation starting from the two single-mode waveguides originated from the two input single-mode waveguides. (b) Detail of the excitation section, where the BC-SMWs and DC-SMWs transfer power to the TE_{00} and TE_{04} modes. (c) Detail of the propagating field in the sensing area of the device. Reproduced with permission from Isayama, Y.H. and Hernández-Figueroa, H.E., published by Sensors, 2021.

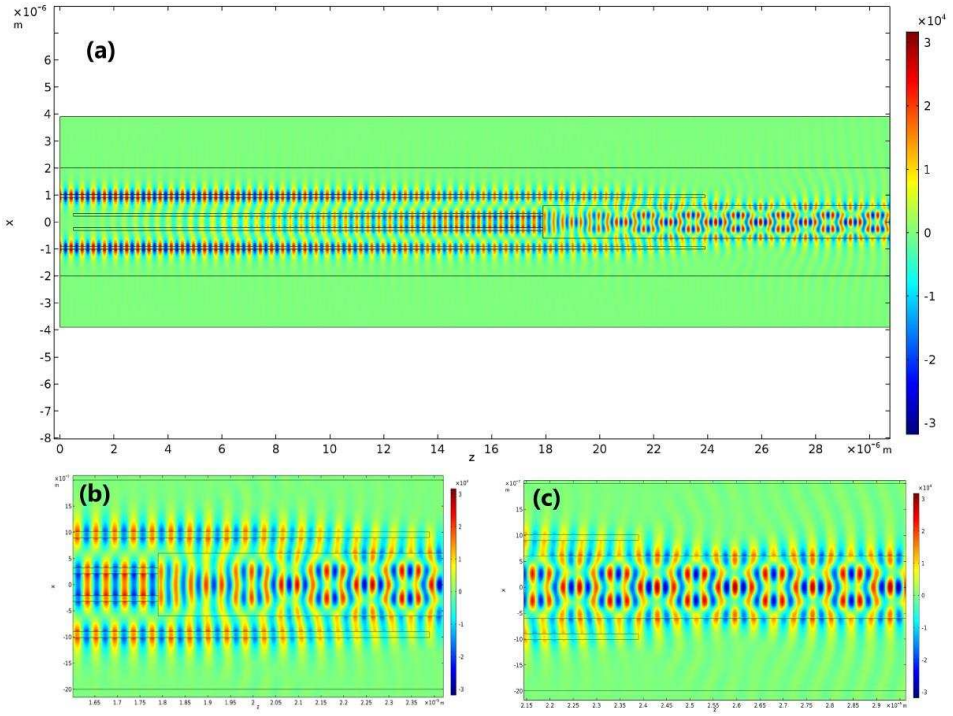

Source: ISAYAMA, Y. H.; HERNÁNDEZ-FIGUEROA, H.E. High-order multimode waveguide interferometer for optical biosensing applications. Sensors, v. 21(9), 2021.

4. DETECTION METHODS

Signal detection and interpretation for MMI sensors have some different possibilities: measuring the output signal directly from the MMW or connecting an output single-mode waveguide after the MMW section and measuring the power coupled to this waveguide. The signal obtained directly from the MMW output will require some postprocessing whereas the output signal from a single-mode waveguide can be interpreted directly.

4.1. SINGLE-MODE WAVEGUIDE OUTPUT

If the chosen detection method is the single-mode waveguide output, as depicted in Figure 4, we have the following relation:

$$d = \sum_{n=0}^{N} c_n e^{-j\beta_n L} \frac{\iint_S \mathbf{e_n}\times\mathbf{H_n}\cdot d\mathbf{S}}{\iint_S \mathbf{E}\times\mathbf{H}\cdot d\mathbf{S}}, \quad (9)$$

where $|d|^2$ is the power fraction at the output of the interferometric device. It represents an

interferometric signal that can be directly related to changes in the sensing area, since perturbations on the cladding region will produce variations in β_n. The total phase ($\beta_n L$) accumulated by each propagating mode inside de MMI will vary and, thus, the amount of optical power coupled to the output waveguide will also be different. Therefore, the measured output power is a function of the material in the sensing area.

4.2. MULTIMODE WAVEGUIDE OUTPUT

If we choose to measure the optical power exiting the multimode section directly, the information must be postprocessed. The information about the accumulated phase for each mode will be present in the EM field distribution obtained. For instance, if we consider a BiMW, which operates with the first order mode, it is known that this mode presents two power peaks. By measuring the output power with two photodiodes, one for each half of the multimode waveguide cross section, the phase difference, $\Delta\phi = \Delta\beta L$, between the modes can be determined by (DUVAL, D. *et al*., 2012)

$$S\,[\%] = \frac{I_{up} - I_{down}}{I_{up} + I_{down}} \times 100\% \qquad (10)$$

$$S(t) \propto \cos\left(\Delta\phi(t)\right) \qquad (11)$$

Where I_{up} and I_{down} are the currents generated in each photodiode and the sensor signal S is proportional to the phase difference $\Delta\phi$ (which, in turn, is related to the refractive index of the sensing area).

As the MMI sensor order gets higher than two, the EM field distribution at the output of the MMI becomes more and more complex. For example, a 4^{th} order MMI sensor requires five photodiodes to measure the output signal, which must be positioned where the five peaks of the 4^{th} order mode are located (ISAYAMA, Y. H.; HERNÁNDEZ-FIGUEROA, 2021)

$$S = \frac{4}{11}\left[\left(\cos^2\frac{\pi}{5} - \cos^2\frac{2\pi}{5}\right) + 2\left(\cos\frac{\pi}{5} - \cos\frac{2\pi}{5}\right)\cos\Delta\phi\right]. \qquad (12)$$

The sensor signal S is proportional to $\cos\Delta\phi$ and can still be used to establish the relationship with refractive index changes in the cladding in the same way as before.

5. EXPERIMENTAL DEMONSTRATION OF A TRIMODAL SENSOR

Over the last years, MMI sensors were mostly investigated and employed as biosensors or refractive index sensors for fluids. However, there has been an interesting demonstration of its application as a temperature sensor as well, using polymeric waveguides, as shown in Figure 6 (RAMIREZ *et al.*, 2019). The device utilizes step junctions at the input and output of the MMI and excites the second order TE mode, which makes this a TriMW sensor. The input power is inserted in the chip through a lensed fiber and the output power is measured at the end of a single-mode waveguide.

A sample interferometric signal obtained from the device with single-mode section width of 3.5μm and trimodal section width of 10.5 μm is shown in Figure 7a. In this configuration the coupling efficiency to the fundamental and second-order modes are 77% and 13%, respectively, which results in a signal visibility of about 5.8 dB and a free spectral range (FSR) of 20.3 nm.

The sensitivity of an interferometric sensor will depend strongly on the visibility of the signal and the FSR reached by the photonic component, by guaranteeing a small FSR and high visibility, a highly sensitive device will be obtained. Variations in the width of the trimodal section can be controlled to improve visibility or free spectral range depending on whether the detection method is based on power measurement, wavelength tuning, or a combination of both, as shown in Figure 7b.

A sample interferometric signal obtained from the device with single-mode section width of 3.5μm and trimodal section width of 10.5μm is shown in Figure 7a. In this configuration the coupling efficiency to the fundamental and second-order modes are 77% and 13%, respectively, which results in a signal visibility of about 5.8 dB and a free spectral range (FSR) of 20.3 nm.

The high order mode interferometer was tested as a temperature sensing device to probe its sensitivity. By varying the temperature from 22°C up to 27°C, it was possible to observe changes in the resulting interferometric signal as shown in Figure 8. By adjusting a line to the measured transmission data at 1486 nm the obtained temperature sensitivity was 0.059 dB/°C. This value is twice as high as

those found in the state-of-the-art for compact and low-loss fiber optical sensors (SUN, Q. *et al.*, 2015).

Figure 7 – Fabrication and characterization system of the trimodal interferometer device. (a) The SEM image of a trimodal device, highlighting the single- and multimode area and the step junction section, respectively. (b) The experimental setup for the trimodal interferometers. (c) Design of the experimental setup to characterize the manufactured interferometric devices.

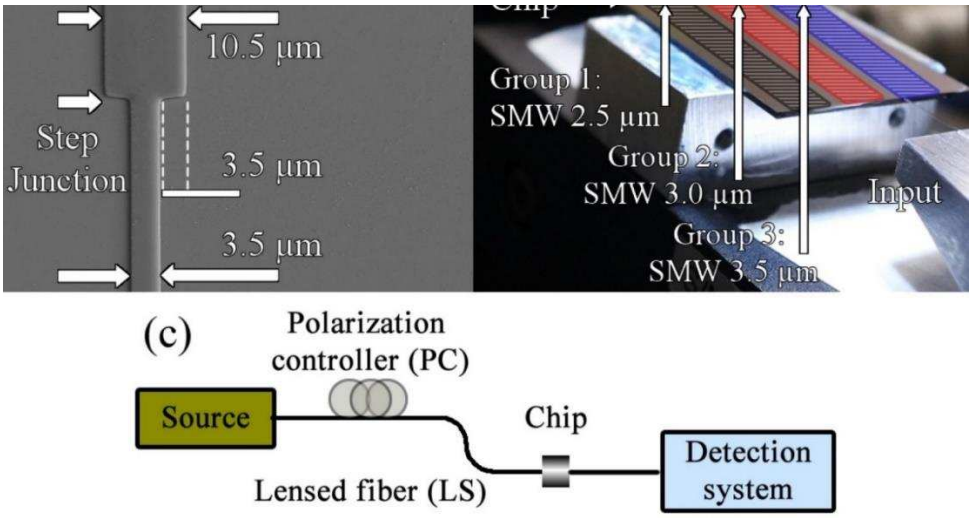

Source: RAMIREZ, J. C. et al. Trimodal waveguide demonstration and its implementation as a high order mode interferometer for sensing application. Sensors (Basel), v. 19, n. 12, p. 2821, 6 2019. Reproduced with permission from Ramirez, J. C., published by Sensors, 2019.

Figure 8 – Sensitivity measurement in trimodal devices. (a) Measured interferometric signal resulting from the modal interaction within a trimodal interferometer with 3.5µm width in the single-mode section and 10.5µm width in the multimodal region. (b) FSR and visibility analysis for a trimodal interferometric device with 600nm height and cross-section with single-mode section width of 3.5µm and variable multimode section width between 10µm and 12µm, with a 0.5µm pitch.

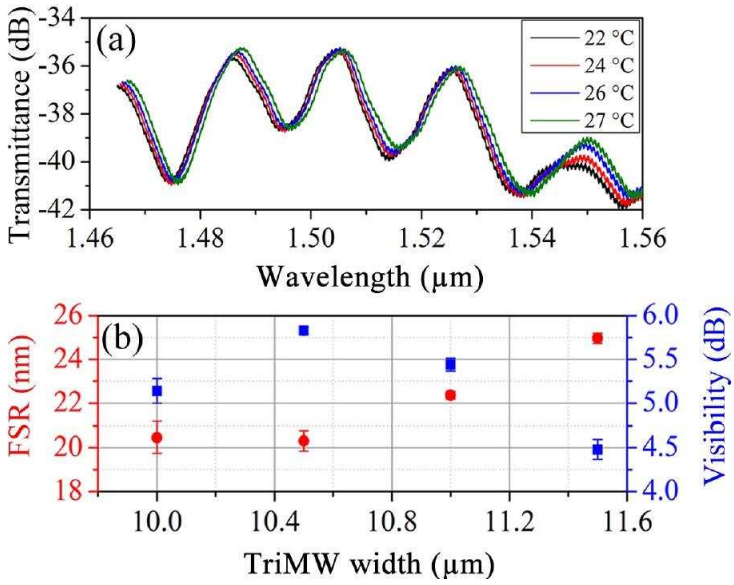

Source: RAMIREZ, J. C. et al. Trimodal waveguide demonstration and its implementation as a high order mode interferometer for sensing application. Sensors (Basel), v. 19, n. 12, p. 2821, 6 2019. Reproduced with permission from Ramirez, J. C., published by Sensors, 2019.

Figure 9 – Fringe power measured as function of temperature variation at 1485nm wavelength peak. Reproduced with permission from Ramirez, J. C., published by Sensors, 2019.

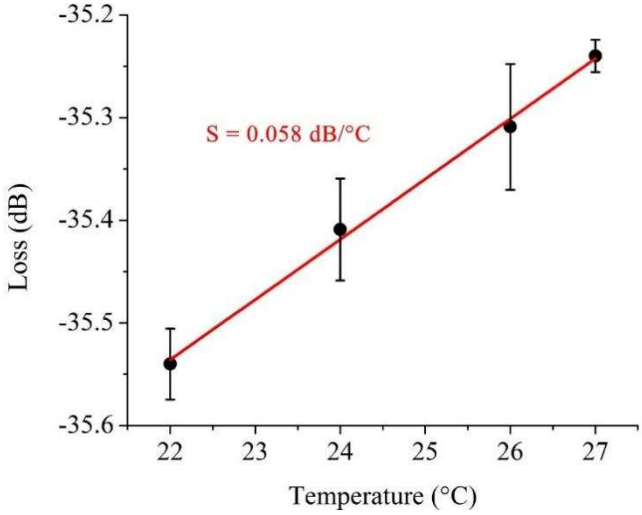

Source: RAMIREZ, J. C. et al. Trimodal waveguide demonstration and its implementation as a high order mode interferometer for sensing application. Sensors (Basel), v. 19, n. 12, p. 2821, 6 2019.

6. CONCLUSIONS AND FINAL REMARKS

In this chapter, the theory about the operation of MMI sensors was presented. There are three structures to be designed or determined: multimode section, excitation structures and detection method. The design of the multimode section consists of choosing a MMI sensor order (i.e. determining what will be the highest order mode supported by the multimode waveguide) and then optimizing the multimode waveguide core geometry (width and height) to maximize device sensitivity. This can be achieved by balancing two aspects of the MMI: increasing the fundamental mode confinement while keeping the high order mode EM field distribution concentrated on the sensing area. The excitation scheme can be chosen to be simpler in terms of construction (step transition) or to be more efficient but complex (BC-SMW and DC-SMW). There are two basic options for the detection method: single-mode output, with simpler detection equipment and interpretation, or multimode output, with more sophisticated measuring schemes and postprocessing.

An experimental demonstration of a TriMW operating as a temperature sensor was also presented. MMI sensors can be built with low-cost materials, such as polymers, and still present good sensitivity characteristics, 0.058 dB/°C at room temperature. Furthermore, the sensitivity obtained is even higher than state-of-the-

art compact low-loss fiber optic sensors, suggesting that MMI sensors could potentially be a viable candidate for other applications as well, such as biosensing.

Even though a large amount of research has been performed regarding MMI sensing and biosensing, there are still many future works and possibilities for the area. With advances in fabrication technologies, new materials or a different composition of materials still need further investigation, as well as different waveguide types and geometries (slot, subwavelength grating, plasmonic, among others). The recent focus was mostly in biosensing applications, but the MMI sensor has shown its merits in terms of sensitivity and capacity for integration, rendering it an interesting option in the most varied types of sensing applications.

ACKNOWLEDGEMENTS

This work was supported by the Brazilian Agencies CAPES and CNPq. The latter under Projects N° 465757/2014-6 (INCT FOTONICOM) and N° 312714/2019-2 (HEHF's Research Productivity Grant); and by the São Paulo Research Foundation (FAPESP) under Project "Photonics for Next Generation Internet").

REFERENCES

ANTONIO-LOPEZ, J. E. *et al*. Tunable multimode-interference bandpass fiber filter. Opt. Lett, v. 35, p. 324–326, 2010.

BERRADA, T. *et al.* Integrated Mach–Zehnder interferometer for Bose–Einstein condensates. Nat. Commun. 2013, 4, 2077.

CHILES, J.; FATHPOUR, S. Mid-infrared integrated waveguide modulators based on silicon-on-lithium-niobate photonics. Optica 2014, 1, 350–355. doi:10.1364/OPTICA.1.000350.

CRESPI, A. *et al.* Integrated multimode interferometers with arbitrary designs for photonic boson sampling. Nat. Photonics 2013, 7, 545–549.

DUVAL, D. *et al*. Nanophotonic lab-on-a-chip platforms including novel bimodal interferometers, microfluidics and grating couplers. Lab Chip, The Royal Society of Chemistry, v. 12, p. 1987–1994, 2012.

DWIVEDI, R.; KUMAR, A. A compact and ultra high sensitive RI sensor using modal interference in an integrated optic waveguide with metal under-cladding. Sensors and Actuators B: Chemical, v. 240, p. 1302–1307, 2017.

DWIVEDI, R.; KUMAR, A. Refractive index sensing using silicon-on-insulator waveguide based modal interferometer. Optik, v. 156, p. 961–967, 2018.

EBIHARA, K.; ASAKAWA, K.; SUZUKI, H. Selectively excited bimodal interferometer for highly sensitive refractive index sensing. Optical Engineering, v. 60, n. 2, p. 027103, 2021.

EBIHARA, K. *et al*. Trimodal polymer waveguide interferometer for chemical sensing. Japanese Journal of Applied Physics, IOP Publishing, v. 58, n. 6, p. 062005, Jun. 2019.

ELSAYED, M. Y. et al. Integrated lab-on-a-chip sensor using shallow silicon waveguide multimode interference (mmi) device. Proceedings Volume 10106, Integrated Optics: Devices, Materials, and Technologies XXI, v. 101060X, 2017.

ESTEVEZ, M.; ALVAREZ, M.; LECHUGA, L. Integrated optical devices for lab-on-a-chip biosensing applications. Laser Photonics Rev. 2012, 6, 463–487. doi:10.1002/lpor.201100025.

FANDIÑO, J.S.; MUÑOZ, P. Photonics-based microwave frequency measurement using a double-sideband suppressed-carrier modulation and an InP integrated ring-assisted Mach–Zehnder interferometer filter. Opt. Lett. 2013, 38, 4316–4319. doi:10.1364/OL.38.004316.

GAVELA, A. F. *et al*. Last advances in silicon-based optical biosensors. Sensors, v. 16, n. 3, 2016.

GONZÁLEZ-GUERRERO, A. B. *et al*. Direct and label-free detection of the human growth hormone in urine by an ultrasensitive bimodal waveguide biosensor. J. Biophotonics, v. 1, p. 61–67, 2017.

GRAJALES, D. *et al*. Low-cost vertical taper for highly efficient light in-coupling in bimodal nanointerferometric waveguide biosensors. J. Phys. Photonics, v. 1, p. 025002, 2019.

GUT, K. *et al*. Applicability of interference te0-tm0 modes and te0-te1 modes to the construction of waveguide sensors. Optica Applicata, v. 29, p. 101–110, 1999.

HOPPE, N. *et al.* Design of an integrated dual-mode interferometer on 250 nm silicon-on-insulator. IEEE Journal of Selected Topics in Quantum Electronics, v. 23, n. 2, p. 444–451, 2017.

ISAYAMA, Y. H.; HERNÁNDEZ-FIGUEROA, H.E. High-order multimode waveguide interferometer for optical biosensing applications. Sensors, v. 21(9), 2021.

KOZMA, P. *et al.* Integrated planar opticalwaveguide interferometer biosensors: A comparative review. Biosens. Bioelectron. 2014, 58, 287–307. doi:10.1016/j.bios.2014.02.049.

KRIBICH, K. R. *et al*. Novel chemical sensor/biosensor platform based on optical multimode interference (mmi) couplers. Sensors and Actuators B: Chemical, v. 107, p. 188–192, 2005.

LEUTHOLD, J.; JOYNER, C. W. Multimode interference couplers with tunable power splitting ratios. Journal of Lightwave Technology, v. 19, n. 5, p. 700–707, 2001.

LEUTHOLD, J. *et al*. Spatial mode filters realized with multimode interference couplers. Opt. Lett., v. 21, p. 836–838, 1996.

LEUTHOLD, J. *et al.* Multimode interference couplers for the conversion and combining of zero- and first-order modes. Journal of Lightwave Technology, v. 16, n. 7, p. 1228–1239, 1998.

LIANG, Y. *et al.* Investigation of grating-assisted trimodal interferometer biosensors based on a polymer platform. Sensors, v. 18, n. 5, 2018. ISSN 1424-8220.

MALDONADO, J. *et al*. Ultrasensitive label-free detection of unamplified multidrugresistance bacteria genes with a bimodal waveguide interferometric biosensor. Diagnostics, v. 10, 2020.

MEHTA, A.; MOHAMMED, W.; JOHNSON, E. G. Multimode interference-based fiber-optic displacement sensor. IEEE Photonics Technology Letters, v. 15, n. 8, p. 1129–1131, 2003.

MOHAMMED, W. S.; MEHTA, A.; JOHNSON, E. G. Wavelength tunable fiber lens based on multimode interference. Journal of Lightwave Technology, v. 22, n. 2, p. 469–477, 2004.

MOHAMMED, W. S.; SMITH, P. W. E.; GU, X. All-fiber multimode interference bandpass filter. Opt. Lett, v. 31, p. 2547–2549, 2006.

RAMIREZ, J. C. *et al.* Trimodal waveguide demonstration and its implementation as a high order mode interferometer for sensing application. Sensors (Basel), v. 19, n. 12, p. 2821, 6 2019.

RAMIREZ, J. C. *et al*. Study of a low-cost trimodal polymer waveguide for interferometric optical biosensors. Opt. Express, OSA, v. 23, n. 9, p. 11985–11994, May 2015.

RASMUSSEN, T.; RASMUSSEN, J. K.; POVLSEN, J. H. Design and performance evaluation of 1-by-64 multimode interference power splitter for optical communications. Journal of Lightwave Technology, v. 13, n. 10, p. 2069–2074, 1995.

SOLDANO, L. B. *et al*. Planar monomode optical couplers based on multimode interference effects. Journal of Lightwave Technology, v. 10, n. 12, p. 1843–1850, 1992.

SOLDANO, L. B.; PENNINGS, E. C. M. Optical multi-mode interference devices based on self-imaging: principles and applications. Journal of Lightwave Technology, v. 13, n. 4, p. 615–627, 1995.

Sun, Q. *et al.* Multimode microfiber interferometer for dual-parameters sensing assisted by Fresnel reflection. Opt. Express 2015, 23, 12777–12783. doi:10.1364/OE.23.012777.